Magnetic source parameters of two-dimensional structures using extended Euler deconvolution

Article *in* Geophysics · May 2001

DOI: 10.1190/1.1444971

CITATIONS
155

READS
622

4 authors, including:

Alan Barry Reid
University of Leeds
36 PUBLICATIONS **2,436** CITATIONS

SEE PROFILE

GEOPHYSICS, VOL. 66, NO. 3 (MAY-JUNE 2001); P. 814–823, 6 FIGS., 2 TABLES.

Magnetic source parameters of two-dimensional structures using extended Euler deconvolution

Martin F. Mushayandebvu*, P. van Driel‡, Alan B. Reid**, and James Derek Fairhead§

ABSTRACT

The Euler homogeneity relation expresses how a homogeneous function transforms under scaling. When implemented, it helps to determine source location for particular potential field anomalies. In this paper, we introduce an additional relation that expresses the transformation of homogeneous functions under rotation. The combined implementation of the two equations, called here extended Euler deconvolution for 2-D structures, gives a more complete source parameter estimation that allows the determination of susceptibility contrast and dip in the cases of contact and thin-sheet sources. This allows for the structural index to be correctly chosen on the basis of a priori knowledge about susceptibility and dip. The pattern of spray solutions emanating from a single source anomaly can be attributed to interfering sources, which have their greatest effect on the flanks of the anomaly. These sprays follow different paths when using either conventional Euler deconvolution or extended Euler deconvolution. The paths of these spray solutions cross and cluster close to the true source location. This intersection of spray paths is used as a discriminant between poor and well-constrained solutions, allowing poor solutions to be eliminated. Extended Euler deconvolution has been tested successfully on 2-D model and real magnetic profile data over contacts and thin dikes.

INTRODUCTION

The use of Euler deconvolution as an interpretation method applied to potential fields (gravity and magnetic) for source depths and location is well established (Reid, 1995). Thompson (1982) developed the technique and applied it to profile data, while, Reid et al. (1990) followed up a suggestion in Thompson's paper and developed the extension to gridded data.

Most of the recent developments in the technique have addressed the issue of cleaning up the solution space by identifying and removing weakly constrained solutions which tend to generate sprays of individual solutions emanating from the clustered, robust solutions (e.g., Fairhead et al., 1994; Kuttikul, 1995; Barbosa et al., 1999). The estimation of the structural index, which relates to source type (e.g., contact, dike, and point) and controls the fall-off rate of the field with distance from the source, is also addressed by Barbosa et al. (1999). Depth estimates are biased if the wrong index is assumed.

These technical issues of poor solutions, structural index, and depth biasing together with the failure of the method to estimate source susceptibility contrast and dip has resulted in the Euler method not being fully accepted as an interpretation method by many potential field users.

With the introduction of an additional rotational constraint, we are able to show that many of the limiting factors on the original Euler method have been overcome and could make extended Euler a method of choice. This contribution restricts itself to the profile method of interpretation of magnetic data and only considers contact and thin dike models. There is no reason why the methodology applied here, suitably modified, cannot be used on profile gravity data and on gridded gravity and magnetic data.

EXTENDED EULER DECONVOLUTION

Extended Euler equation

We denote a 2-D space with depth z (positive down) and horizontal distance x. For a special class of magnetic anomalies, the

Presented at the 69th Annual Meeting, Society of Exploration Geophysicists. Manuscript received by the Editor July 14, 1999; revised manuscript received June 26, 2000.
*Formerly University of Leeds, School of Earth Sciences, Leeds LS2 9JT, U.K.; presently Image Interpretation Technologies Inc., 2010, 520-5th Avenue, S.W., Calgary, Alberta T2P 3R7, Canada. E-mail: martin@iitech.ab.ca.
‡Shell International Exploration and Production B. V., Research and Technical Services, EPT-GA, Volmerlaan, P.O. Box 60, 2280 AB Rijswijk, The Netherlands. E-mail: p.vandriel@siep.chell.com.
**Formerly GETECH, c/o University of Leeds, School of Earth Sciences; presently Reid Geophysics, 49 Carr Bridge Dr., Leeds LS16 7LB, U.K. E-mail: alan@reid-geophys.co.uk.
§GETECH, c/o University of Leeds, School of Earth Sciences, Leeds LS2 9JT, U.K. E-mail: jdf@getech.leeds.ac.uk.

potential is a homogeneous function of order n of the distance r; where $r^2 = z^2 + x^2$ in the 2-D plane. Under scaling $r \to e^{\lambda} r$, which transforms the potential $M \to e^{-n\lambda} M$ so that M satisfies

$$(x - x_o)\frac{\partial M}{\partial x} + (z - z_o)\frac{\partial M}{\partial z} = -NM. \tag{1}$$

This equation is the 2-D Euler equation, with N defined as the structural index. If the structural index of the source is known, its depth and location (x_o, z_o) can be determined.

When homogeneous functions are also invariant under rotations $r \to e^{i\lambda} r$, they transform the potential $M \to e^{-ni\lambda} M$. This invariance leads to

$$(x - x_o)\frac{\partial M}{\partial z} - (z - z_o)\frac{\partial M}{\partial x} = 0. \tag{2}$$

As an example, for fields which decay from source as

$$M(x - x_o, z - z_o) = \frac{C}{r^N}, \tag{3}$$

where C is a constant associated with the physical properties of the source and $r^2 = (x - x_o)^2 + (z - z_o)^2$, the gradients of the fields are

$$\frac{\partial M}{\partial x} = -N(x - x_o)\frac{C}{r^{N+2}} = -NM\frac{(x - x_o)}{r^2}, \tag{4}$$

$$\frac{\partial M}{\partial z} = -N(z - z_o)\frac{C}{r^{N+2}} = -NM\frac{(z - z_o)}{r^2}. \tag{5}$$

Hence, multiplying equation (4) by $(x - x_o)$ and equation (5) by $(z - z_o)$ and adding gives the Euler equation. Multiplying equation (4) by $(z - z_o)$ and equation (5) by $(x - x_o)$ and subtracting gives the rotational constraint. We show that for particular solutions this leads to equations that allow one to solve for additional source parameters such as dip and susceptibility.

Magnetic contact

The equations for the magnetic field (M) and its associated derivatives for a contact extending to depth with its top edge at (x_o, z_o), are given by Nabighian (1972). For the derivatives,

$$\frac{1}{\alpha}\frac{\partial M}{\partial z} = \frac{(x - x_o)\cos(\beta) + (z - z_o)\sin(\beta)}{r^2} \tag{6}$$

and

$$\frac{1}{\alpha}\frac{\partial M}{\partial x} = \frac{(x - x_o)\sin(\beta) - (z - z_o)\cos(\beta)}{r^2}, \tag{7}$$

where $\alpha = 2KFc\sin(d)$, $\beta = 2I - d - 90^\circ$ for the total field anomaly, and $r^2 = (z - z_o)^2 + (x - x_o)^2$ with K the susceptibility contrast at the contact, d the local dip, F the magnitude of the earth's magnetic field, $c = 1 - \cos^2(i)\sin^2(A)$ for i the ambient field inclination and A the angle between the magnetic north and the x-axis, and $\tan(I) = \tan(i)/\cos(A)$. Substituting these into equations (1) and (2) leads to

$$(x - x_o)\frac{\partial M}{\partial x} + (z - z_o)\frac{\partial M}{\partial z} = \alpha\sin(\beta) \tag{8}$$

and

$$(x - x_o)\frac{\partial M}{\partial z} - (z - z_o)\frac{\partial M}{\partial x} = \alpha\cos(\beta). \tag{9}$$

Equations (8) and (9) are extensions of the Euler equation for the magnetic contact, which theoretically has a structural index of zero.

Equation (8) is implemented by Reid et al. (1990), who solve for the right-hand side of the equation as an offset whose value combines amplitude, strike, and dip effects. By also implementing equation (9), the right-hand sides of the two equations now give two equations with two unknowns; hence, one can solve for α and β. If the geomagnetic field strength and its inclination and declination are known, one can solve for the dip of the contact and the susceptibility, assuming there is no remanent magnetization. Solving equations (8) and (9) jointly for the least-squares estimates of the source location using the Moore–Penrose inversion (Lawson and Hanson, 1974) or equivalent techniques puts additional constraints on the Euler solutions.

Thin dike

The equation for the magnetic field of a thin dike extending to depth with its top edge at (x_o, z_o) is the horizontal derivative of the field for a magnetic contact (Nabighian, 1972) and is given by

$$\frac{M}{\alpha} = \frac{(x - x_o)\sin(\beta) - (z - z_o)\cos(\beta)}{r^2}, \tag{10}$$

with α now equal to $2KFct\sin(d)$ where t is the thickness of the dike. The other terms have the same definitions as for the magnetic contact. The derivatives are

$$\frac{1}{\alpha}\frac{\partial M}{\partial x}(x, z) = \frac{-2(x - x_o)[(x - x_o)\sin(\beta) - (z - z_o)\cos(\beta)]}{r^4} + \frac{\sin(\beta)}{r^2}, \tag{11}$$

$$\frac{1}{\alpha}\frac{\partial M}{\partial z}(x, z) = \frac{-2(z - z_o)[(x - x_o)\sin(\beta) - (z - z_o)\cos(\beta)]}{r^4} - \frac{\cos(\beta)}{r^2}. \tag{12}$$

Substituting these into equations (1) and (2) gives

$$(x - x_o)\frac{\partial M}{\partial x} + (z - z_o)\frac{\partial M}{\partial z} = -M \tag{13}$$

and

$$(x - x_o)\frac{\partial M}{\partial z} - (z - z_o)\frac{\partial M}{\partial x} = -\frac{\alpha}{r^2}[(x - x_o)\cos(\beta) + (z - z_o)\sin(\beta)] = -V. \tag{14}$$

Equation (13) is the conventional Euler equation for a thin dike with a structural index of 1. Interestingly in equation (14) V is the vertical gradient of the magnetic field from the magnetic contact [equation (6)]. Since V is not known, equation (13) is used to determine the source location, and equation (14) is then used to determine V.

Its easy to show that

$$M^2 + V^2 = \frac{\alpha^2}{r^2}, \tag{15}$$

$$(z - z_o)V + (x - x_o)M = \alpha \sin(\beta), \tag{16}$$

$$(x - x_o)V - (z - z_o)M = \alpha \cos(\beta). \tag{17}$$

Thus, the dip and the product of the susceptibility contrast and the thickness can be determined if the field strength and inclination are known and assuming there is no remanent magnetization. Since M and V are the horizontal and vertical derivatives, respectively, of the field over an equivalent contact coinciding with the dike, equations (16) and (17) show the same relationships as equations (8) and (9), the extended Euler equations for a magnetic contact.

SOLUTION STRATEGY AND MODEL STUDIES

The methodology for the implementation of Euler deconvolution is described well by Reid et al. (1990); extended Euler deconvolution follows the same approach. Application of extended Euler deconvolution is illustrated using isolated dipping magnetic contact and thin dike models. These give exact solutions from all data windows for the source location, the dip, the susceptibility or the product of the susceptibility, and the thickness for the case of the dike, independent of the window size (e.g., Figure 1 and Table 1).

Extended Euler deconvolution has also been implemented successfully on models with interfering sources—for example, thick dikes (Figure 2) which are taken to represent close contacts and multiple dikes (Figure 3). The synthetic anomalies are not contaminated with noise. In the figures, unless stated otherwise in the caption, all Euler source locations below the surface are presented. A structural index of 0 is used for the contact and 1 for the dike models. Though the source characteristics are well estimated at points where there is a tight clustering of Euler solutions, the figures illustrate the typical spraying of solutions because of source interference effects, window location relative to the anomaly, etc. The interference effects for the close contacts (dike 2, Figure 2) result in shallower depth and less steep source dip estimates than the true model, with susceptibility contrasts still well estimated.

A number of techniques are available to distinguish between robust and poorly constrained Euler solutions, e.g., applying an acceptance criterion based on the scatter in the estimated depths (Thompson, 1982), applying a Laplacian filter to limit the Euler method to portions of the grid which show significant curvature (Fairhead et al., 1994), using the positive curvature of the analytic signal as an acceptance criterion (Kuttikul, 1995), and only selecting solutions that produce the best fit to known quantities, such as a combination of the anomaly and its gradients (Barbosa et al., 1999). Extended Euler deconvolution allows a further technique for removing the poorly constrained solutions.

For a contact, the spraying of Euler solutions emanating from the true source location follows different paths, depending on whether equation (8) (conventional Euler), equation (9) (the rotational constraint), or both are used to invert the source

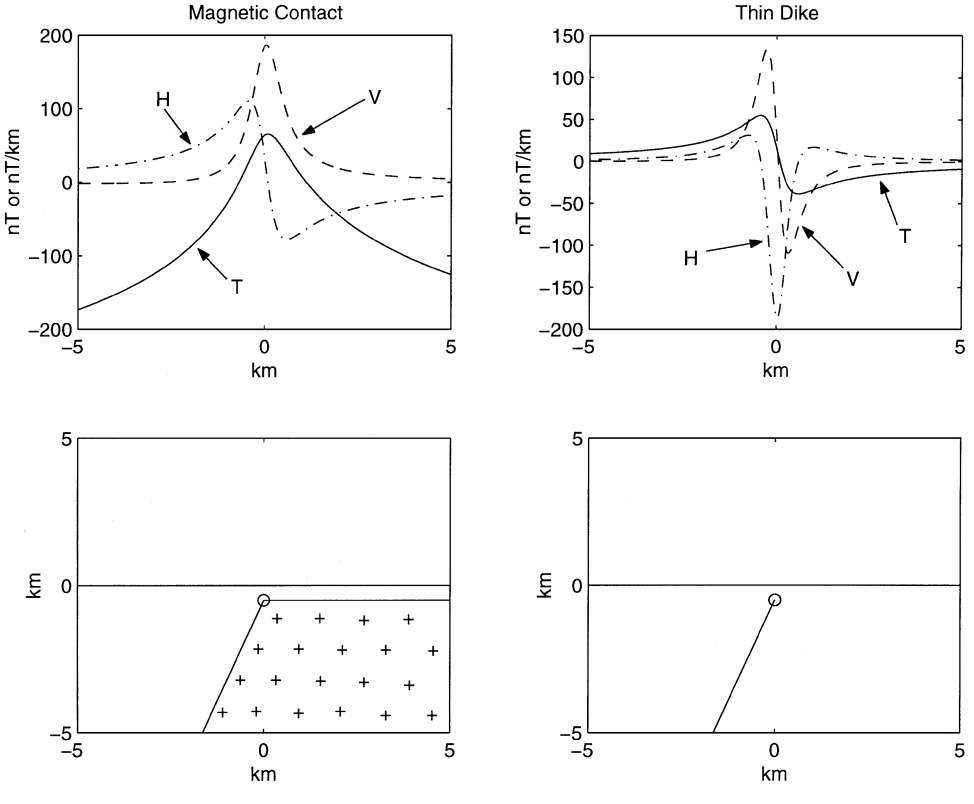

FIG. 1. Total magnetic field and gradients over a contact and a thin dike with the associated models derived from extended Euler deconvolution [solid—total field (T); dashed and dotted—horizontal gradients (H); dashed—vertical gradients (V)]. Geomagnetic field characteristics: 50,000 nT field strength, inclination 60°. Susceptibility contrasts are given in Table 1.

location. The solutions cluster tightly, and the spray paths cross close to the source location. In this way, when the intersection of these paths is determined, the spray is reduced drastically. This approach removes the sprays as demonstrated in Figure 2 by accepting only solutions from equation (8) by itself and equations (8) and (9) simultaneously, which agree at some acceptance level. A similar approach is used to clean out the spraying for thin dikes (Figure 3).

A step-by-step description of the implementation procedures is summarized below, and Table 1 summarizes the results obtained. An Euler window of 10 points (i.e., 450 m long) was used. The errors obtained depend on the degree of cleaning out of the sprays and are quoted as ± 1 standard deviation.

The determination of the structural index in the case of contacts and prisms depends on the knowledge of the dip and the susceptibility. Extended Euler deconvolution allows for the structural index to be correctly chosen on the basis of a priori knowledge about the susceptibility and the dip.

Implementation procedure for contacts.—For a given window, first use conventional Euler deconvolution, with a structural index $N = 0$ to solve equation (8) by a least-squares method for source location (x_o, z_o). Let depth1 $= z_o$. Figure 2f shows conventional Euler deconvolution solutions.

Second, use extended Euler deconvolution to solve equations (8) and (9) simultaneously for source location (x_o, z_o), α, and β which allows the determination of dip and susceptibility contrasts. The value z_o now equals depth2. Figures 2c–e show extended Euler deconvolution solutions.

Finally Compute the relative difference in depth, $[(|\text{depth2} - \text{depth1}|)/\text{depth2}] \times 100\%$. If the difference is less than the acceptance level chosen by the user (e.g., 10%), depth2, dip, and susceptibility are kept; otherwise, they are rejected. Figures 2g–i show extended Euler deconvolution solutions after cleaning out the solution space.

Implementation procedure for thin dikes.—For a given window, first use conventional Euler deconvolution with a structural index $N = 1$ to solve equation (13) by a least-squares method for source location (x_o, z_o). Let depth3 $= z_o$. Figure 3c shows conventional Euler deconvolution solutions.

Second, Knowing (x_o, z_o), use equation (14) to solve for V, the vertical gradient of the equivalent contact.

Third, solve Equations (15) and (16) or (17) simultaneously for α and β, which allows for the determination of dip and susceptibility contrasts × thickness product of the thin dike. Figures 3d,e show extended Euler deconvolution solutions.

Fourth, using the observed magnetic field M and the computed field V (corresponding to the horizontal and vertical gradients of the magnetic field because of the equivalent contact) and conventional Euler equation (8) with $N = 0$, estimate the location of the equivalent contact (x_o, z_o). Now z_o equals depth4. Figure 3f shows the locations of the equivalent contact.

Finally, compute the relative difference in depth, $[(|\text{depth4} - \text{depth3}|)/\text{depth3}] \times 100\%$. If the difference is less than the acceptance level chosen by the user (e.g., 10%), depth4, dip, and susceptibility*thickness product are kept; otherwise, they are rejected. Figures 3g–i show the extended Euler deconvolution solutions after cleaning out the solution space.

APPLICATION TO REAL DATA

The application of extended Euler deconvolution to real data is illustrated using a 25-km-long aeromagnetic data profile over the Great Dyke of Zimbabwe which targets shallow sources and then using a 350-km-long profile across the Teisseyre–Tornquist zone (TTZ) in Poland looking at deeper sources. Figure 4a shows a west–east magnetic profile over the Great Dyke. A brief description of the geology and the data as well as the results from the profile are discussed below to illustrate the use of extended Euler deconvolution.

Figure 5a shows a representative magnetic profile across central Poland from southwest to northeast. The figure illustrates how the extended Euler deconvolution solutions can be used to build a starting 2-D model for forward modeling.

Great Dyke of Zimbabwe

Brief geology.—The formation of the Archaean Zimbabwe craton was the culmination of events during the time span circa 2900–2600 Ma (Wilson, 1990). The intrusion of the Great Dyke at 2461 ± 16 Ma (Hamilton, 1977) was the first major igneous event after cratonization. The dike is 550 km long and up to 11 km wide and extends in a north–northeast-trending direction from the Limpopo Belt in the south into the Zambezi Belt in the north. The Great Dyke is not a true dike, but at its present erosion level it is the remains of a number of elongated synclinally layered mafic igneous complexes emplaced along a line of weakness in the earth's crust (Wilson and Prendergast, 1988). The sequences pass downward into true dike feeders

Table 1. Modeling results ± one standard deviation. Values in brackets are the true model parameters being inverted for. All the model dikes have a thickness of 100 m.

Model		Number of solutions	Euler depth (m)	Susceptibility (SI units) [× thickness (m) for dikes]	Dip (degrees)
Dike		All windows	500 ± 0 (500)	6.3 ± 0 (6.3)	110 ± 0 (110)
Contact		All windows	500 ± 0 (500)	0.126 ± 0 (0.126)	110 ± 0 (110)
Thick dikes (modeled as contacts)					
Dike 1	Left edge	8	530 ± 80 (500)	0.086 ± 0.005 (0.063)	125 ± 10 (120)
	Right edge	13	475 ± 45 (500)	−0.056 ± 0.013 (−0.063)	67 ± 8 (70)
Dike 2	Left edge	6	350 ± 40 (500)	0.12 ± 0.02 (0.126)	133 ± 5 (110)
	Right edge	9	480 ± 150 (500)	−0.16 ± 0.05 (−0.126)	55 ± 4 (80)
Multiple dikes (numbered from left to right)					
Dike 1		24	520 ± 40 (500)	9 ± 2 (12.6)	120 ± 4 (140)
Dike 2		27	520 ± 40 (500)	20 ± 2 (18.9)	74 ± 3 (80)
Dike 3		10	480 ± 10 (500)	11 ± 1 (12.6)	106 ± 4 (100)
Dike 4		13	490 ± 15 (500)	8 ± 1 (12.6)	66 ± 14 (55)

to the complexes (Podmore and Wilson, 1987). Each complex consists of a lower ultramafic sequence and an upper mafic sequence with each sequence consisting of layered cyclic petrogenetic units. Layering in the cyclic units plunges gently toward the center of each complex. The mafic sequence has been entirely removed by erosion and is only preserved in the center of the synclines. The ultramafic sequence contains dunites, harzburgites, olivine-bronzitites, pyroxenites, and thin layers of chromite.

Running nearly parallel to the Great Dyke for its entire length are its main satellites, the Umvimeela dike (to the west) and the East dike (to the east). These are composed of quartz gabbros and were correlated with the Great Dyke by Worst (1960). McElhinny and Gough (1963) and Jones et al. (1975) confirm this relationship with their palaeomagnetic results. The satellites are generally undeformed except for relatively small offsets associated with a number of cross-cutting faults. They are, however, extensively deformed at the northern end within the Zambezi Belt. The satellite dikes are essentially vertical with a mean dip of 84° toward the Great Dyke for the Umvimeela dike and 89° away from the Great Dyke for the East dike, with average widths of 200 m and 100 m, respectively (Mushayandebvu, 1995).

Magnetic data.—The whole of Zimbabwe has been covered by an aeromagnetic survey program funded by the Canadian Development Agency, implemented in three phases. The Great Dyke and its satellites were covered by the first phase, carried

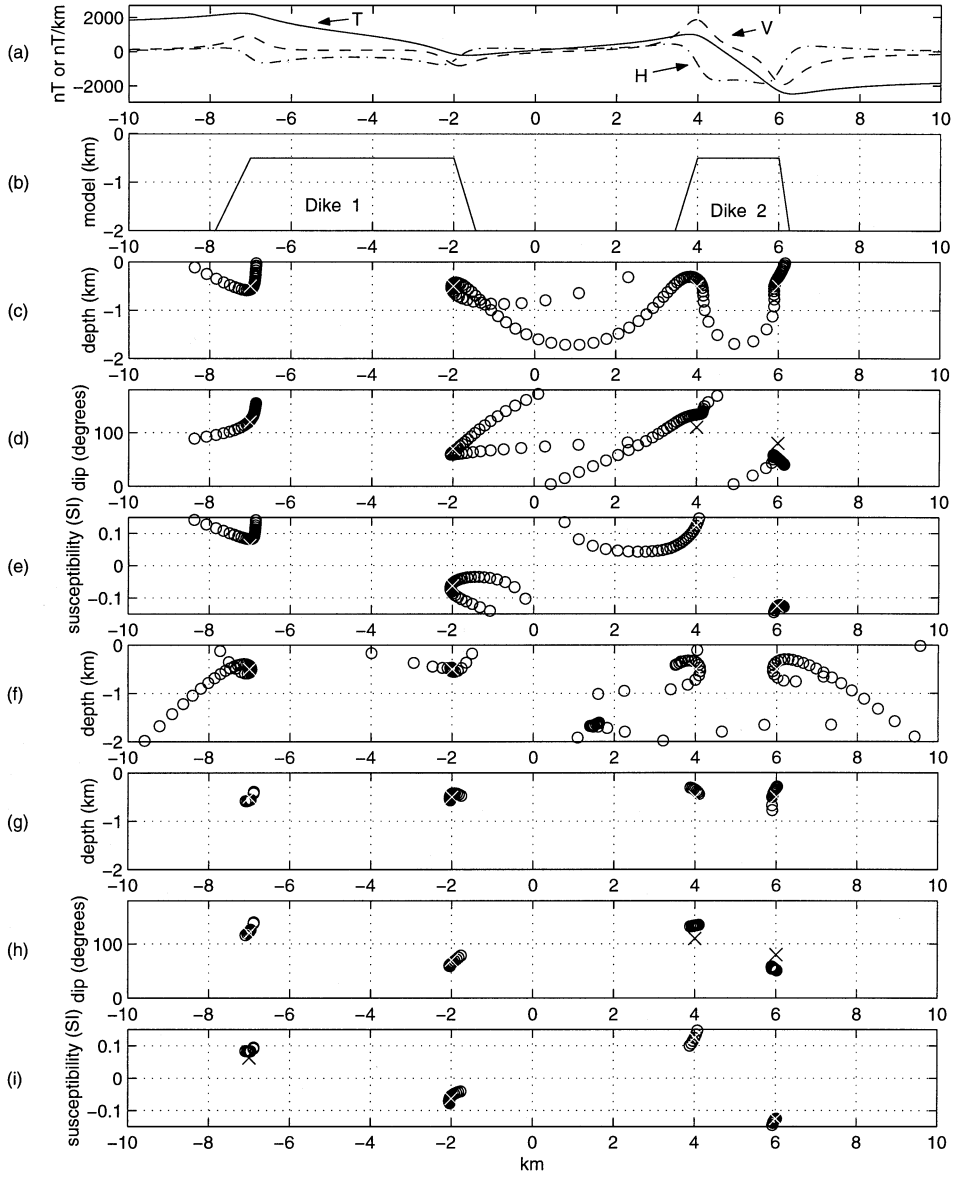

FIG. 2. Extended Euler deconvolution solutions from magnetic profiles (a) (same code and units as in Figure 1) over thick dikes modeled as contacts (b). Model source characteristics being inverted for are marked with an *X*. Solutions obtained from a combined use of conventional Euler [equation (8)] and the rotational constraint [equation (9)] are presented: depths in kilometers (c), dip in degrees (d), and the susceptibility contrast (e) with a few points plotting outside the plot window. Solutions for conventional Euler [using equation (8)] are presented in (f). Cleaning of spraying by using a 10% agreement in depth estimates is presented in (g), (h), and (i), maintaining the same units. Geomagnetic field characteristics: 50,000 nT field strength, inclination 60°.

out in 1983 by Kenting Earth Sciences Ltd., which covered the central third of the country. The survey was carried out at a mean terrain clearance of 305 m with east–west traverse lines spaced 1 km apart and north–south tie lines every 14 km. Total magnetic field data were obtained using a proton magnetometer with a resolution of 0.25 nT.

Remanent magnetization is often a complication in magnetic interpretation. For the Great Dyke and its satellites, the component of the remanence in the plane perpendicular to the dike is very close in direction to that of the present geomagnetic field. The direction of the remanent magnetization in the Umvimeela dike is declination $(D) = 219.8^\circ$, inclination $(I) = -58.7^\circ$, and a circle of 95% confidence around that direction, or $\alpha_{95} = 3.3^\circ$ (Mushayandebvu, 1991). In the Great Dyke, $D = 220.4^\circ$, $I = -58.3^\circ$, and $\alpha_{95} = 8.2^\circ$ (McElhinny and Gough, 1963). The geomagnetic field has an inclination of -55° and a declination of -10°. The dike anomalies could be modeled as the result of remanent and induced magnetization or as fully induced. If the magnetization is assumed to be induced, then higher susceptibilities are required to produce the observed anomalies.

Deconvolution.—The extended Euler deconvolution was run with a structural index of 0 to identify contacts. Then it was run with a structural index of 1 to identify dikes. No attempts were made to find intermediate structural indices which might

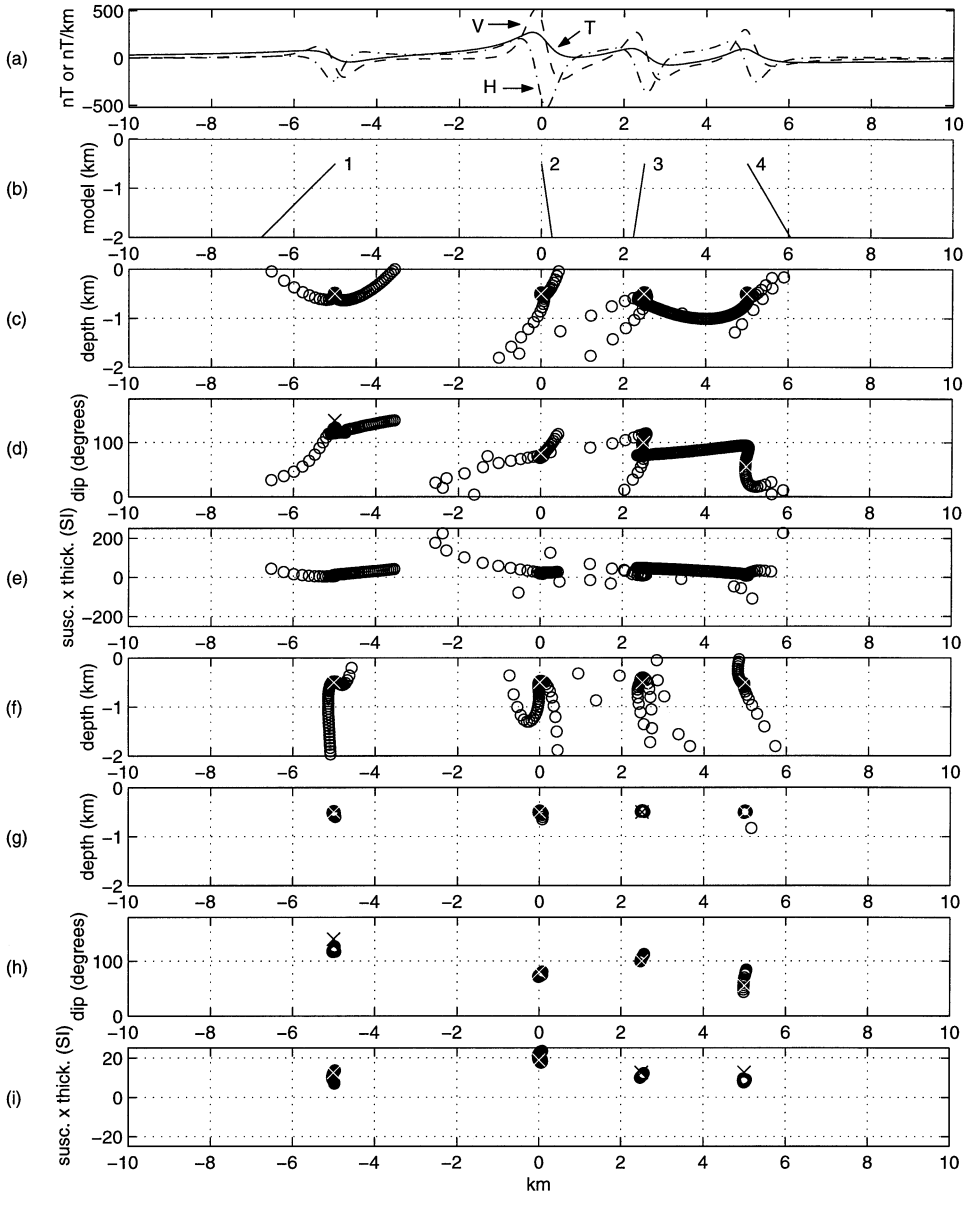

FIG. 3. Extended Euler deconvolution solutions from magnetic profiles (a) (same code and units as in Figure 1) over multiple thin dike models (b). Model source characteristics being inverted for are marked with an *X*. All solutions from extended Euler deconvolution are presented: depths in kilometers (c), dip in degrees (d), and the product of the susceptibility contrast and the thickness (e) with a few points plotting outside the plot windows. Solutions for the equivalent magnetic contacts are presented in (f). Cleaning of spraying by using a 10% agreement in depth estimates is presented in (g), (h), and (i), maintaining the same units. Geomagnetic field characteristics: 50,000 nT field strength, inclination 60°.

improve solution clustering but are not related to a known model structure. The results for the dikes and the contacts are presented together (Figure 4). Besides the conventional clustering of solutions, the dip and susceptibility contrast associated with the chosen model can help in assessing the suitability of the choice. When structures are not well defined, it is possible to have both the dike and contact models identifying source points with different depths (contact depths tend to be shallower). In many cases, it is now possible to choose the more appropriate model from the clustering of the associated dip and susceptibility values. It is also now possible to choose the correct structural index on the basis of a priori knowledge about the susceptibility and the dip. The deconvolution was run using a number of window sizes. The choice is always a trade-off between reducing noise in data, which needs larger window sizes, and reducing source interference, which needs smaller windows.

The profile (Figure 4a) is a 25-km section of a flight line which cuts the Great Dyke at 17.48°S latitude and runs west to east. An estimate of the strike of the Great Dyke was made from aeromagnetic maps, and the profile data were projected onto a profile perpendicular to the dike before deconvolution. This gave a mean sampling interval of 66 m. The results obtained from using a window size of 20 points (1.25 km long) are presented. The same acceptance criteria described in the earlier section on Solution Strategy and Model Studies are applied but using an acceptance criterion of 15% agreement in depths.

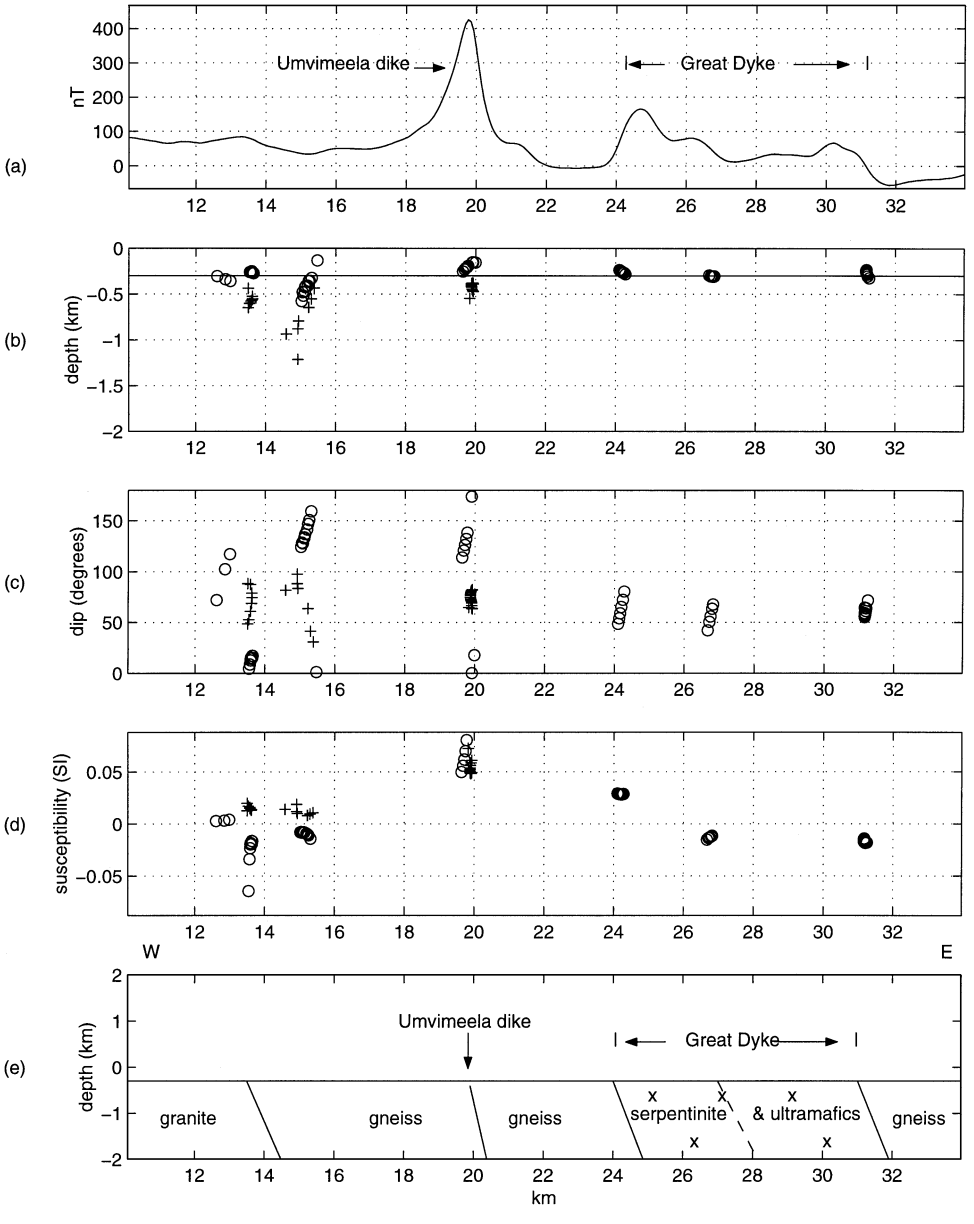

FIG. 4. Extended Euler deconvolution solutions from a magnetic profile over the Great Dyke, Zimbabwe: (a) total field magnetic profile, (b) depth (kilometers) (ground level marked), (c) dip (degrees), (d) susceptibility contrast (SI units) (for contacts) or product of the susceptibility and the thickness (for dikes) (kilometers). The + symbols are solutions from inversion using the dike model (structural index of 1); the circles are solutions from using the contact model (structural index of 0). A simplified geological section from the interpretation is given (e). (Profile provided by Geological Survey of Zimbabwe.)

Isolated solutions have been rejected. The depths (Figure 4b) are from the flight height, so they must be reduced by 305 m (the flight height) for depth from the surface. The dips (Figure 4c) are defined as an angle from the positive x-direction, varying from 0° to 180°.

The Umvimeela dike stands out with the largest anomaly centered near the 20-km marker on the profile. When inverted with a structural index of 1, i.e., assuming it is a dike, it comes out with a depth to the top from the flight height of 410 ± 50 m, a dip of $73^\circ \pm 6^\circ$, and a product of susceptibility and thickness of 53 ± 6 m (SI units) This agrees well with the expected mean value of $84^\circ \pm 12^\circ$ for the dip. Hand specimens from the Umvimeela dike give a mean susceptibility of 0.008 (SI units) and a product of susceptibility and thickness of 1.6 m (SI units) (Mushayandebvu, 1995). This value is much less than the value obtained from Euler deconvolution, which indicates the anomalous field is predominantly from remanence. Inverted as a contact, i.e., using a structural index of zero, the depth to the top of the contact would be above the ground with a larger scatter in the dip estimates, showing the dike model as the preferred model.

The Great Dyke signature is a lower amplitude but broader anomaly which stretches from the 24-km to 31-km markers. The complex nature of this layered intrusion is evident in the magnetic response and the variations in solutions with different window sizes. The Great Dyke comes out as three contacts. The westernmost contact has a dip of $63^\circ \pm 12^\circ$ and a susceptibility contrast of 0.029 ± 0.005 (SI units). The easternmost contact has a similar dip of $62^\circ \pm 5^\circ$ with a susceptibility contrast of -0.016 ± 0.003 (SI units), the negative sign indicating a drop in susceptibility with increasing distance in the positive profile direction. A contact is also mapped inside the dike with a dip of $56^\circ \pm 10^\circ$ and a susceptibility of -0.013 ± 0.001 (SI units). Interference between these closely spaced edges affects the dip estimates. The edges identified by the inversion are steeper than the layering of the cyclic petrogenetic units within the dike and are hence assumed to represent the structure of the weathered near-surface serpentinite zone.

A low-amplitude anomaly near the 14-km marker can be seen. This roughly coincides with the mapped contact between gneissic and granitic terrains. Extended Euler deconvolution shows the contacts, which crop out with dips of $16^\circ \pm 2^\circ$. The strike of the contacts is not accurately known, but a rough estimate gives a strike correction that would increase the dip to about 60°. Although granite can produce significant magnetic anomalies, a large intrusive body that cooled slowly tends to have large magnetite grains as magnetic remanence carriers which do not hold a stable remanence (Spall and Noltimier, 1972). As a result, the observed magnetic anomaly can be assumed to be predominantly induced. A simplified geological section derived from the extended Euler solutions is presented in Figure 4e.

Teisseyre–Tornquist Zone, Poland

Brief geology.—Poland can be subdivided into three broad geological units: the Precambrian East European platform to the northeast, the younger and mobile Paleozoic West European platform to the southwest, and an area of Alpine folding to the south. The boundary between the East European

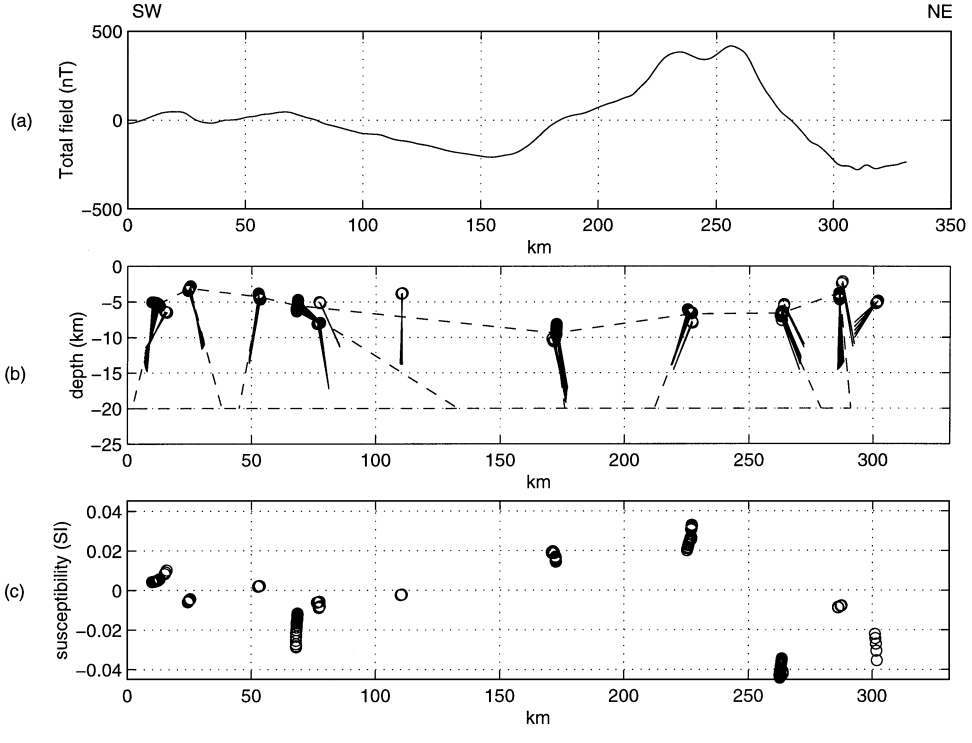

FIG. 5. Extended Euler deconvolution solutions from a magnetic profile across the Teisseyre–Tornquist zone, Poland. (a) Total field magnetic profile. (b) Solution depths (kilometers) from a flight height of 500 m and dips using a structural index of 0 for contacts (depths are marked with circles, and dips are marked with a line from the circle), with the dashed outline marking a simplified geological section used in forward modeling (Figure 6). (c) Susceptibility contrast.

and West European platforms is known as the Teisseyre–Tornquist zone (TTZ), which trends northwest–southeast through central Poland. The East European platform is a stable block where Paleozoic and Mesozoic deposits are essentially unaffected by any orogenic phases. The West European platform underwent folding and faulting during Variscan and Alpine orogenies and developed a thick sequence of Paleozoic and Mesozoic deposits. The TTZ is Europe's longest tectonic lineament that bisects the continent in a northwest–southeast direction from the North Sea to the Black Sea. Its width through Poland varies between 50 km in the northwest to 90 km in the southeast (Guterch et al., 1986). The TTZ exhibits major deformation, which has affected both the basement and overlying sediments. No volcanic rocks appear to be present; thus, the smooth nature of the southwest–northeast magnetic profile (Figure 5a) reflects magnetic basement at depths of 3 to 6 km, substantiated by seismic data (Śledziński, 1998). The distribution of mineral deposits in Poland is controlled by the TTZ, with most being situated southwest of this feature.

Magnetic data.—The profile has been constructed by Geophysical Exploration Technology Ltd. from a national compilation of mainly total intensity ground data processed using a 500-m grid spacing with a 500-m terrain clearance. The positive anomaly centered on 250 km is a major magnetic anomaly paralleling the northeast side of the TTZ and is clearly delineated by Magsat crustal data (Taylor and Ravat, 1995).

Deconvolution.—The extended Euler deconvolution was run with a structural index of 0 to identify magnetic contacts

Table 2. Extended Euler solutions across the Teisseyre–Tornquist zone picking up contacts. Errors are ± one standard deviation.

Location (km)	Number of solutions	Depth (km)	Dip (degrees)	Susceptibility contrasts (SI units)
12.2 ± 1.6	20	5.4 ± 0.5	121 ± 13	0.0054 ± 0.0020
24.9 ± 0.3	10	3.1 ± 0.2	56 ± 5	−0.0050 ± 0.0006
53.0 ± 0.2	11	4.3 ± 0.3	114 ± 1	0.0025 ± 0.0005
68.4 ± 0.2	25	5.5 ± 0.4	15 ± 3	−0.018 ± 0.005
77.1 ± 0.5	3	8.0 ± 0.1	66 ± 3	−0.0063 ± 0.0005
77.5 ± 0.2	4	5.1 ± 0.1	37 ± 1	−0.0085 ± 0.0005
110.4 ± 0.2	4	3.8 ± 0.0	91 ± 3	−0.0025 ± 0.0005
172.1 ± 0.6	31	9.4 ± 0.8	63 ± 3	0.017 ± 0.002
226.5 ± 0.6	23	6.7 ± 0.5	136 ± 3	0.026 ± 0.003
263.1 ± 0.4	34	6.6 ± 0.4	41 ± 3	−0.040 ± 0.003
286.5 ± 0.6	8	3.7 ± 1.0	80 ± 12	−0.0085 ± 0.0006
301.6 ± 0.3	5	5.1 ± 0.1	157 ± 4	−0.028 ± 0.005

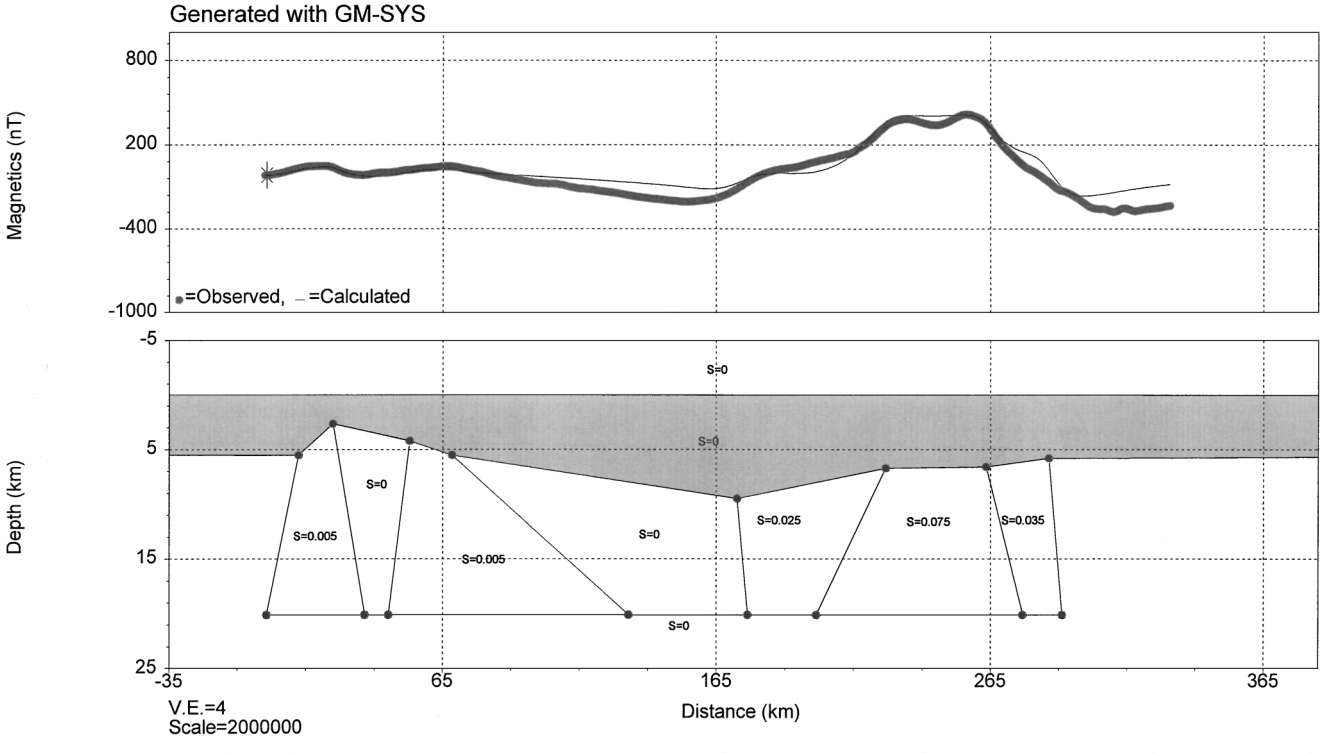

FIG. 6. Forward modeling using of extended Euler deconvolution solutions from a magnetic profile across the Teisseyre–Tornquist zone, Poland, Northwestern Geophysical Associates' Modeling software, GM-SYS.

with a window size of 60 points (15 km long). The data have been projected onto a profile perpendicular to the TTZ before carrying out the deconvolution. The results are presented in Figure 5. An acceptance criterion of 20% agreement in depths was used, and isolated solutions were rejected. The depths presented (Figure 5b) are relative to a 500-m mean terrain clearance since the grid used had been upward continued by that amount to unify the various ground and airborne surveys. Table 2 gives the mean values and associated errors for the source parameters for each of the solution clusters. The dip information has been incorporated into the depth sections, with the circles marking the source locations and the line emanating from the source location showing the dip angle. The contacts identified have been interpreted to represent changes in rock type with a smooth basement rather than faults; thus, the profile maps the thickness of the sediments. For a detailed geological correlation of the gravity and magnetic field with the main geological units, refer to Śledziński (1998).

A simple, geological, smooth basement model has been built from the Euler solutions (Figure 5b). An assumed initial depth to the bottom of the model is 20 km. Mean values of the source locations and dips given in Table 2 have been used. Assigning susceptibilities to the different units is more problematic since extended Euler devolution only provides susceptibility contrasts at contacts. We have used the averages of the increases on one side of a magnetic unit and the decreases on the other to estimate initial susceptibilities. The section produced has provided the starting model for forward modeling using Northwestern Geophysical Associates' modeling software GM-SYS (Figure 6) and produces a reasonable initial fit. No attempt has been made to iterate the forward model to improve the fit.

CONCLUSION

Extended Euler deconvolution combines the Euler homogeneity relation and a relation that stems from the transformation of homogeneous functions under rotation. When applied to magnetic contact models, it improves the determination of the source location and allows for the determination of the dip and susceptibility contrast. When applied to thin dike models, it allows for the determination of the dip and the product of susceptibility contrast and thickness. The added information is used to correctly choose the structural index on the basis of prior knowledge about the susceptibility and dip. The spray pattern of solutions follows different paths when using either conventional Euler deconvolution or extended Euler deconvolution for both contact and dike models. The paths cross and the solutions cluster close to the source location. In this way, when the intersection of these paths is determined, the spray is drastically reduced, enabling more reliable estimates of source location and associated parameters.

ACKNOWLEDGMENTS

The authors thank Shell International Exploration and Production B.V. for allowing the publication of this work. The research was funded through a fellowship granted by the British National Environment Research Council to JDF under the Realizing Our Potential award scheme and held by MFM. We thank A. H. Saad (Associate Editor), J. B. C. Silva, E. K. Biegert, and an anonymous reviewer for their comments which led to substantial improvements in the paper.

REFERENCES

Barbosa, V. C. F., Silva, J. B. C., and Medeiros, W. E., 1999, Stability analysis and improvement of structural index estimation in Euler deconvolution: Geophysics, **64**, 48–60.

Fairhead, J. D., Bennet, K. J., Gordon, D. R. H., and Huang, D., 1994, Euler: Beyond the "Black Box": 64th Ann. Internat. Mtg., Soc. Expl. Geophys., Expanded Abstracts, 422–424.

Guterch, A., Grad, M., Materzok, R., and Perchuc, E., 1986, Deep structure of the Earth's crust in the contact zone of the Paleozoic and Precambrian platforms of Poland (Tornquist-Teisseyre Zone), *in* Galson, D. A., and Muller, S., Eds., The European geotraverse, Part 2: Tectonophys, **128**, 251–279.

Hamilton, J., 1977, Sr isotope and trace element studies on the Great Dyke and Bushveld mafic phase and their relationship to early Proterozoic magma genesis in southern Africa: J. Petr., **18**, 24–52.

Jones, D. L., Robertson, I. D. M., and McFadden, P. L., 1975, A palaeomagnetic study of Precambrian dyke swarms associated with the Great Dyke of Rhodesia: Trans. Geol. Soc. S. Afr., **78**, 57–65.

Kuttikul, P., 1995, Optimization of 3D Euler deconvolution for the interpretation of potential field data: M.S. thesis, Internat. Training Centre, Delft.

Lawson, C. L., and Hanson, R. J., 1974, Solving least squares problems: Prentice-Hall, Inc.

McElhinny, M. W., and Gough, D. I., 1963, The palaeomagnetism of the Great Dyke of southern Rhodesia: Geophys. J., **7**, 287–303.

Mushayandebvu, M. F., 1991, A palaeomagnetic study of mafic intrusions associated with the Great Dyke, Zimbabwe: Ph.D. thesis, Univ. Zimbabwe.

—— 1995, Magnetic modelling of the Umvimeela and East dykes: Evidence for regional tilting of the Zimbabwe craton adjacent to the Limpopo Belt: J. Appl. Sci. in S. Afr., **1**, 47–58.

Nabighian, M. N., 1972, The analytic signal of two-dimensional magnetic bodies with polygonal cross-sections: Its properties and use for automated anomaly interpretation: Geophysics, **37**, 507–517.

Podmore, F., and Wilson, A. H., 1987, A reappraisal of the structure, geology and emplacement of the Great Dyke, Zimbabwe, *in* Halls, H. C., and Fahrig, W. F., Eds., Mafic dyke swarms: Geol. Assoc. Canada, Spec. Paper 34, 317–330.

Reid, A. B., 1995, Euler deconvolution: Past, present and future, a review: 65th Ann. Internat. Mtg., Soc. Expl. Geophys., Expanded Abstracts, 272–273.

Reid, A. B., Allsop, J. M., Granser, H., Millett, A. J., and Somerton, I. W., 1990, Magnetic interpretation in three dimensions using Euler deconvolution: Geophysics, **55**, 80–91.

Śledziński, J., 1998, Geotectonics and geodynamics of the Teisseyre–Tornquist tectonic zone: Warsaw University of Technology Reports on Geodesy, **34**, No. 4.

Spall, H., and Noltimier, H. C., 1972, Some curious magnetic results from a Precambrian granite: Geophys. J. Roy. Astr. Soc., **28**, 237–248.

Taylor, P. T., and Ravat, D., 1995, An interpretation of the Magsat anomalies of central Europe: Appl. Geophys., **34**, 83–91.

Thompson, D. T., 1982, EULDPH—New technique for making computer-assisted depth estimates from magnetic data: Geophysics, **47**, 31–37.

Wilson, J. F., 1990, A craton and its cracks: Some of the behaviour of the Zimbabwe block from the late Archaean to the Mesozoic in response to horizontal movements, and the significance of some of its mafic dyke fracture patterns: J. Afr. Earth Sci., **10**, 483–501.

Wilson, A. H., and Prendergast, M. D., 1988, The Great Dyke of Zimbabwe—1: Tectonic setting, stratigraphy, petrology, structure, emplacement and crystalization, *in* Prendergast, M. D., and Jones, M. J., Eds., Magnetic sulphides—The Zimbabwe volume. Inst. Min. Metal., 1–20.

Worst, B. G., 1960, The Great Dyke of southern Rhodesia: S. Rhodesia Geol. Surv. Bull., **47**.